Lattice Boltzmann scheme for crystal growth in external flows

Dmitry Medvedev* and Klaus Kassner
Otto-von-Guericke University, Postfach 4120 D-39016 Magdeburg, Germany
(Received 7 June 2005; published 9 November 2005)

A composite phase-field lattice-Boltzmann scheme is used to simulate dendritic growth from a supercooled melt, allowing for heat transport by both diffusion and convection. The phase-transition part of the problem is modelled by the phase-field approach of Karma and Rappel, whereas the flow of the liquid is computed by the lattice-Boltzmann-BGK (LBGK, referring to Bhatnagar, Gross, and Krook) method into which interactions with solid and thermal convection are incorporated. For simplicity, we have so far restricted ourselves to the symmetric model. Heat transport is simulated via the multicomponent LBGK method. Depending on the level of anisotropy and undercooling, dendrites or doublons are obtained in our simulations. Crystal growth in a shear flow is considered for different flow velocities and undercoolings. Doublons turn out to be robust against the perturbation imposed by a shear flow and display interesting dynamic behavior, quite different from that of dendrites. In addition, the influence of a parallel flow on the operating state of the tip of dendrites is studied. To complement information from selection theories such as the one presented by Bouissou and Pelcé, we measure selected growth characteristics of dendrites as a function of a flow imposed parallel to the growth direction, for intermediate undercoolings. The observed dependencies are compatible with power law behavior, if the undercooling is not too high. It is shown that for sufficiently large flow velocities, an oncoming flow can lead to tip oscillations of the dendrite and, consequently, to the generation of coherent side branches.

DOI: 10.1103/PhysRevE.72.056703 PACS number(s): 02.70.−c, 68.08.−p, 68.70.+w

I. INTRODUCTION

Dendritic patterns are the most ubiquitous microstructures arising in the solidification of melts. Their size, composition, and orientation distribution determine the macroscopic mechanical properties of materials obtained in casting such as strength, hardness, and ductility. While the basic mechanism of dendritic growth has been understood for some time in terms of microscopic solvability [1–5], the relevance of this understanding for practical applications has been impaired by the fact that only rarely are conditions met that permit a direct quantitative comparison with the theoretical description. Ordinarily, this description refers to a situation at small undercooling and without convection. Because in most real-life situations convection is inevitable, a better understanding of dendritic growth in the presence of flow in the melt is an important theoretical and practical problem, notwithstanding the desirability of experiments testing the current theory via creation of conditions with as little convection as possible.

Some years ago, the long-standing observation of the existence of structures besides the dendritic one (the "dense-branching" morphology [6]) was put on a firmer theoretical basis [7]: Scaling arguments and asymptotic analysis were used to postulate a kinetic phase diagram [7,8], comprising, in addition to the regular compact dendritic structure, fractal dendrites as well as the compact and fractal seaweed morphologies. Later the theory was modified [9] in a way that established doublons as the basic building blocks of the seaweed morphology. None of these theoretical developments considered convection. In particular, it was completely unknown how convection would affect doublon structures or, for that matter, whether this structure, where a pair of asymmetric fingers stabilize one another, would survive in a flow at all.

However, there have been various attempts at an analytic description of dendritic growth itself under certain flow conditions, with somewhat inconclusive results. Earlier approaches [10–13] just extended the Ivantsov solution [14], neglecting surface tension effects, to situations with simple flow fields, essentially forced flow in the Oseen approximation and potential flows (see also Ref. [15]). Descriptions involving an element of selection theory were developed by Bouissou and Pelcé [16], by Ben Amar and Pomeau [17], as well as by Ananth and Gill [18], the last authors assuming simply that the selection parameter is not influenced by convection. This way the only difference in comparison with selection theory without flow is a change in the relationship between the Péclet number and the undercooling. The slightly more sophisticated theories by Bouissou and by Ben Amar, on the other hand, partially contradict each other, the former claiming that a stationary needle crystal cannot exist beyond a certain velocity of the imposed flow, the latter giving steady-state results for arbitrary flow velocities. Nevertheless, the theories proposed in Refs. [13,16] seem compatible with experiments on dendritic growth in an imposed flow [19,20].

Under normal growth conditions, i.e., if we do not have a microgravity setup, the inhomogenous temperature distribution in the solidification sample will produce thermal convection. Even under microgravity, the density difference between the two phases induces convection. Effects of convective flows on the characteristic growth parameters of dendrites (tip radius and tip velocity) were indeed suggested to have been observed at low undercoolings in microgravity experiments [21]. On the other hand, alternative explanations

*Corresponding author. Fax: +49-0391-6711205. Email address: Dmitry.Medvedev@physik.uni-magdeburg.de

for these observations such as proximity effects of the walls were also proposed [22]. Nevertheless, it is clear that at least under gravity, natural convection can substantially influence the growth process and the features of the resulting pattern. A theoretical approach to this case of free convection has been suggested by Sekerka *et al.* [23].

A number of attempts to numerically simulate crystal growth in the presence of convection have been put forward recently. Juric [24] used a finite-difference front-tracking method to investigate microstructure formation under fluid flow. More recently, the phase-field method has become the method of choice for simulations of dendritic solidification. Its main advantage is the absence of the need of front tracking, together with the possibility of keeping good accuracy at moderate computational cost, if a thin-interface approach such as the one discussed by Karma and Rappel [25,26] is employed. In the framework of this setting, first simulations of convection in dendritic growth have been performed [27–29] in diverse geometries and with both imposed flows and natural convection. With all of these methods, the solution of the Navier-Stokes equations is time consuming, because fluid incompressibility has to be ensured.

At this point, it is useful to recall that the lattice-Boltzmann (LB) method is presently a well-established tool to simulate fluid flows, especially flows in complex geometries [30,31]. It can be easily modified to account for the thermal transport due to convection and diffusion, and buoyancy forces can also be incorporated without any problems. Other advantages of the method are its good stability and the ease of parallelization.

Therefore it seems natural to combine phase-field and lattice-Boltzmann approaches for simulations of dendritic growth in external flows. One attempt in this direction was made in Ref. [32], others in Refs. [33–35]. Our model is similar, but it is simpler in the LB part (at least in two dimensions, where $2\times 9=18$ distribution functions are used instead of 24, and the collision matrix is simpler) and more consistent in the phase-field part.

The motivation of the combination lies in its promise of improved efficiency, allowing us to simulate lower undercoolings and hence larger systems with about the same computational effort as necessary even in small systems with the other methods. The idea that the method is promising is, of course, based on the fact that both the phase-field and lattice-Boltzmann approaches have proved to be very efficient in their respective domains of application in the past. Moreover, there is nothing in these approaches nor in their combination that prevents geometric parallelization of large systems—both are completely local methods and their combination does not destroy this property. So we indeed expect computational advantages of the method in the future.

The purpose of this paper is twofold. On the one hand, we wish to establish the viability of the approach combining two of the most advanced simulation techniques, hitherto mainly used in different contexts. On the other hand, we will consider the influence of convection not only on the basic dendritic morphology but also on the doublonic one. The long-term aim will be to describe the morphology diagram including its dependence on parameters quantifying convective flows.

In Sec. II, we discuss the basic model equations, while Sec. III is devoted to the method of their implementation. In Sec. IV, we consider crystal growth into a shear flow, in Sec. V, the external flow is directed parallel to the needle structure and towards its tip. Section VI gives some concluding remarks.

II. SHARP-INTERFACE MODEL

The reference equations for the problem of dendritic growth from a supercooled melt in the presence of a fluid flow with velocity $\mathbf{U}$ are those of the sharp-interface model:

$$\partial_t u + \mathbf{U}\,\boldsymbol{\nabla}\, u = D\nabla^2 u,$$

$$\mathbf{n}\cdot\mathbf{V} = D\mathbf{n}\cdot(\,\boldsymbol{\nabla}\, u|_s - \,\boldsymbol{\nabla}\, u|_l),$$

$$u_i = -\,d(\theta)/R - \beta\mathbf{n}\cdot\mathbf{V}. \tag{1}$$

Herein, $u=c_p(T-T_m)/L$ is the normalized temperature, D the thermal diffusivity, and $\mathbf{n}$ the local normal to the liquid-solid interface. $d(\theta)$ is the capillary length, related to the orientation-dependent interface tension $\gamma(\theta)$ between the solid and its melt by $d(\theta)=(d_0/\gamma_0)[\gamma(\theta)+\gamma''(\theta)]$. θ is the angle between the interface normal and some fixed direction (usually identified with the x axis of the coordinate system), γ_0 the average of the interface tension over all orientations, and $d_0=\gamma_0 T_m c_p/L^2$ the similarly averaged capillary length, in which T_m denotes the melting temperature of a flat solid, c_p the heat capacity per unit volume, assumed equal in both phases, and L the latent heat per unit volume. R is the local radius of curvature, β the kinetic coefficient, and $\mathbf{V}$ the interface velocity. In principle, β is orientation dependent, too. However, we will consider the case of fast attachment kinetics here, meaning that β becomes negligible. This implies certain constraints on the choice of parameters of the phase-field model, discussed briefly below. Moreover, we restrict ourselves to the symmetric model with equal densities and thermal diffusivities of solid and liquid phases.

The boundary condition for the normal velocity is often referred to as the Stefan condition, while the last equation in Eq. (1), describing the interface temperature, is the Gibbs-Thomson condition (for $\beta=0$) with kinetic correction (for $\beta\neq 0$).

As equations of motion for the fluid velocity $\mathbf{U}$, we take the Navier-Stokes equations and the continuity equation for an incompressible fluid, which are then supplemented by boundary conditions at the interface,

$$\partial_t\mathbf{U} + \mathbf{U}\,\boldsymbol{\nabla}\,\mathbf{U} = -\frac{\boldsymbol{\nabla}P}{\rho} + \nu\nabla^2\mathbf{U},$$

$$\boldsymbol{\nabla}\cdot\mathbf{U} = 0,$$

$$\mathbf{U}_i = 0, \tag{2}$$

where equal mass densities ρ have been assumed in the two phases, ν is the kinematic viscosity, and P denotes the pressure of the liquid. $\mathbf{U}_i$ is the flow velocity at the interface. The

interface boundary conditions are not the most general ones: if there is a density difference between the liquid and solid phases, it is still reasonable to assume the tangential velocity to be equal to zero at the interface (sticking condition), while the normal velocity is determined by a source term proportional to the density difference. We will not consider this case here.

In addition to the boundary conditions at the interface, far-field boundary conditions have to be required to render the problem well posed. Since these conditions are different for different numerical setups, we will discuss them only when presenting the simulations.

III. METHOD

Having in mind the advantages of the phase-field method in the simulation of crystal growth as well as the virtues of lattice-Boltzmann schemes for flow simulations with complex boundaries, we developed a combination of the two approaches, aiming at a computation of dendritic growth from a supercooled melt in more realistic settings than that of purely diffusive dynamics.

The essential features of our scheme are the following:

(i) Simulation of solidification is accomplished using the phase-field model introduced by Karma and Rappel [25,26].

(ii) The flow of the liquid is simulated by the standard LBGK method [36] with incorporated interactions of the flow with the solid and with buoyancy forces (in the case of thermal convection).

(iii) The conductive and convective heat transfer is computed by a multicomponent LB method similar to the one used in Ref. [37].

Obviously, the second step (flow simulation) can be omitted in the case of purely diffusional growth.

A. Solidification and phase-field method

The phase-field model is written as

$$\tau(\theta)\partial_t\psi = [\psi - \lambda u(1-\psi^2)](1-\psi^2) + \boldsymbol{\nabla}\cdot[W^2(\theta)\,\boldsymbol{\nabla}\,\psi] - \partial_x[W(\theta)W'(\theta)\partial_y\psi] + \partial_y[W(\theta)W'(\theta)\partial_x\psi],$$

$$\partial_t u + \mathbf{U}\,\boldsymbol{\nabla}\,u = D\nabla^2 u + \frac{1}{2}\partial_t h(\psi). \tag{3}$$

The value $\psi=1$ of the phase-field variable corresponds to the solid phase, $\psi=-1$ to the liquid phase. Here, $W(\theta)$ is an anisotropic interface width, $\tau(\theta)$ a relaxation time, and $\theta = \arctan(\partial_y\psi/\partial_x\psi)$ is the angle between the local interface normal and the x axis. The last term in the second equation describes latent heat release during solidification. We used the simplest form $h(\psi)=\psi$, which has been shown to be computationally more efficient [26] than more elaborate expressions.

Via a suitable asymptotic expansion, the equations of a sharp-interface model (1) can be derived [26], with the following expressions for the capillary length and kinetic coefficient:

$$d(\theta) = \frac{I}{\lambda J}[W(\theta) + \partial_\theta^2 W(\theta)],$$

$$\beta(\theta) = \frac{I}{\lambda J}\frac{\tau(\theta)}{W(\theta)}\left(1 - \lambda\frac{K+JF}{2I}\frac{W^2(\theta)}{\tau(\theta)}\right).$$

These equations, derived by Karma and Rappel [25], have been shown to be equivalent to a second-order accurate standard asymptotic approximation [26,38].

In order to obtain a vanishing kinetic coefficient, the following relations must be imposed [25]:

$$W = W_0 A(\theta), \quad \tau = \tau_0 A^2(\theta), \quad \lambda = \frac{2ID\tau_0}{(K+JF)W_0^2}.$$

For our choice of $h(\psi)$, the values of the coefficients are $I = 2\sqrt{2}/3$, $J=16/15$, $K=0.136\,04$,[1] and $F=\sqrt{2}\ln 2$ [25,26]. We use the fourfold anisotropy function

$$A(\theta) \equiv \frac{\gamma(\theta)}{\gamma_0} = 1 + \varepsilon\cos 4\theta,$$

leading to

$$d(\theta) = (1 - 15\ \varepsilon\cos 4\theta)d_0.$$

Moreover, we set $\tau_0=1$, $W_0=1$.

The equation for the phase-field ψ was discretized on a uniform spatial lattice with grid spacing $\Delta x=0.4$, and it was solved using the explicit Euler method with constant time step Δt in the range 0.008–0.016.

B. Lattice-Boltzmann method for flow

To simulate the flow of the liquid and the heat transport, we employ the LBGK method (see Ref. [31]). It uses one-particle distribution functions f_k defined at the nodes of a regular spatial lattice as main variables. Different labels k correspond to different velocities $\mathbf{c}_k$ from a fixed finite set. In the two-dimensional model used here, these velocities are $\mathbf{c}_0=(0,0)$, $\mathbf{c}_k=(\cos[(k-1)\pi/2], \sin[(k-1)\pi])\delta x/\delta t$ for $k=1$, …, 4, and $\mathbf{c}_k=\sqrt{2}(\cos[(k-1/2)\pi/2], \sin[(k-1/2)\pi/2])\delta x/\delta t$ for $k=5$, …, 8. Here, δx is the grid spacing, equal for both directions, δt is the time step. The effect of making the velocities proportional to $\delta x/\delta t$ is that nonzero velocities lead to nearest-neighbor and next-nearest-neighbor sites of the square lattice in one time-step, i.e., only lattice point positions appear in the dynamics, no interpolations are necessary.

Inside the LB part of our simulations, the grid spacing and time step are both formally rescaled to 1, which is the reason why we have used a different notation for them here from that in the phase-field part of the simulation (δx and δt vs Δx and Δt), although they are actually the same "material" quantities.

The evolution equation for f_k is

[1] The exact value is $K=\sqrt{2}(\frac{188}{225}-\frac{16}{15}\ln 2)$.

$$f_k(t+\delta t,\mathbf{x}+\mathbf{c}_k\delta t)=f_k(t,\mathbf{x})+\frac{f_k^{eq}-f_k}{\tau_f}\delta t. \quad (4)$$

Distribution functions are advected (first term on the right-hand side) and undergo a relaxation to equilibrium values f_k^{eq} which are, as usual, taken to be expansions of Maxwellians up to second order in the fluid velocity $\mathbf{U}$,

$$f_k^{eq}=\rho w_k\left(1+\frac{\mathbf{c}_k\cdot\mathbf{U}}{c_s^2}+\frac{(\mathbf{c}_k\cdot\mathbf{U})^2}{2c_s^4}-\frac{U^2}{2c_s^2}\right), \quad (5)$$

with c_s having the physical meaning of an isothermal sound velocity. The local fluid density is given by $\rho=\Sigma_k f_k=\Sigma_k f_k^{eq}$, the flow velocity is $\mathbf{U}=\Sigma_k f_k\mathbf{c}_k/\rho$, and the weight coefficients are $w_0=4/9$, $w_{1-4}=1/9$, $w_{5-8}=1/36$. This form of the equilibrium distribution functions ensures mass and momentum conservation and provides the correct form of the momentum flux tensor [31,36].

Performing a Chapman-Enskog expansion, one can derive from Eq. (4) the continuity and Navier-Stokes equations [31], with kinematic viscosity $\nu=c_s^2(\tau_f-\delta t/2)$. The isothermal sound velocity is $c_s=\delta x/\sqrt{3}\delta t$, for small flow velocities the fluid is almost incompressible (effects of compressibility are proportional to U^2/c_s^2).

The influence of the growing pattern on the fluid flow was simulated as proposed in Refs. [28,29]. An additional dissipative force was introduced in partially filled regions

$$\mathbf{F}_d=-\rho\nu\frac{2g\phi^2}{W_0^2}\mathbf{U},$$

where $g=2.757$ and $\phi=(1+\psi)/2$ is the solid fraction. This provides the correct velocity boundary conditions at the diffuse interface (see Refs. [28,29]), i.e., the sharp-interface limit of the velocity boundary conditions of Eq. (2) is correctly reproduced. The value of the constant g was obtained in Refs. [28,29] by an asymptotic analysis of plane flow past the diffusive interface.

The action of forces on a liquid was simulated by the exact difference method of Ref. [39]. The term $\Delta f_k=f_k^{eq}(\rho,\mathbf{U}+\Delta\mathbf{U})-f_k^{eq}(\rho,\mathbf{U})$ is added to the right-hand side of Eq. (4), where $\Delta\mathbf{U}=\mathbf{F}\delta t/\rho$ is the velocity change due to action of force $\mathbf{F}$ at time step δt. This form of the change of distribution functions is exact in the case where the distribution is equilibrium before the action of the force (then after the action the distribution remains equilibrium), hence the name of the method. In the case of a nonequilibrium initial state, this method is accurate to second order in $\Delta\mathbf{U}$. It is simple enough and valid for arbitrary lattices and any dimension of space.

Also, thermal convection in the liquid can be easily included introducing the buoyancy force in the Boussinesq approximation $\mathbf{F}_c=-\rho\alpha(1-\phi)(T-T_0)\mathbf{g}$, where α is the thermal expansion coefficient and $\mathbf{g}$ the gravitational acceleration, and treating it the same way as other forces.

C. Lattice-Boltzmann method for heat transport

The temperature transport was simulated using a second set of distribution functions N_k. Their evolution equation reads

$$N_k(t+\delta t,\mathbf{x}+\mathbf{c}_k\delta t)=N_k(t,\mathbf{x})+\frac{N_k^{eq}-N_k}{\tau_T}\delta t. \quad (6)$$

Here, $N_k^{eq}=N_k^{eq}(T,\mathbf{U}+\Delta\mathbf{U}/2)$, where $T=\Sigma_k N_k$, $\mathbf{U}=\Sigma_k f_k\mathbf{c}_k/\Sigma_k f_k$, $\Delta\mathbf{U}=\mathbf{F}\delta t/\Sigma_k f_k$, $\mathbf{F}=\mathbf{F}_d+\mathbf{F}_c$ is the total force. The functional form for N_k^{eq}

$$N_k^{eq}=Tw_k\left(1+\frac{\mathbf{c}_k\cdot\mathbf{U}}{c_s^2}+\frac{(\mathbf{c}_k\cdot\mathbf{U})^2}{2c_s^4}-\frac{U^2}{2c_s^2}\right)$$

is the same as for f_k [Eq. (5)], with T instead of ρ. This scheme leads to

$$\frac{\partial T}{\partial t}+\mathbf{U}\,\boldsymbol{\nabla}\,T=\chi\nabla^2 T,$$

the equation for convective and conductive heat transport with constant thermal diffusivity $\chi=c_s^2(\tau_T-\delta t/2)$ (that is, the symmetric model is realized).

To be able to identify χ with the diffusion constant from Eq. (3), we must require $\tau_T/\delta t=1/2+3D\Delta t/\Delta x^2$, where D is the thermal diffusivity. The Prandtl number is therefore $\mathrm{Pr}=\nu/D=(\tau_f/\delta t-1/2)\Delta x^2/3D\Delta t$. In the practical calculation, δt is set equal to 1, or more precisely, Eqs. (4) and (6) contain only the nondimensional combinations $\tau_f/\delta t$ and $\tau_T/\delta t$, respectively (if t and $\mathbf{x}$ are considered mere counter variables for the numbers of time and lattice steps, i.e., $t\hat{=}n$, $t+\delta t\hat{=}n+1$, etc.).

The latent heat production on the right-hand side of Eq. (3) is taken into account by multiplying the distribution functions after propagation and collisions $N_k(t+\delta t)$ [Eq. (6)] by the ratio of the new value of temperature (increased by the latent heat release) to the old one,

$$N_{k\ \mathrm{new}}=N_{k\ \mathrm{old}}\frac{T_{\mathrm{new}}}{T_{\mathrm{old}}}.$$

Here, $T_{\mathrm{new}}=T_{\mathrm{old}}+1/2h_\psi(\psi)\partial_t\psi\Delta t$, and in our case, $h_\psi(\psi)=1$.

When the values of T become small, the scheme works poorly, therefore we used $T=u+\Delta+1.0$, where $\Delta=c_p(T_m-T_0)/L$ is the nondimensional initial undercooling.

An advantage of this method over direct simulations of the diffusion equation (3) is that it is less restrictive concerning the admissible size of the time step. As is well known, for the diffusion equation, stability of an explicit scheme requires the time step Δt to scale as the *square* of the grid spacing Δx. This is a simple consequence of the fact that the diffusion equation is first order in time but second order in space. A propagative scheme such as Eq. (6), which is first order both in time and space, allows one to choose time steps that scale linearly with the grid spacing. This will always lead to an advantage of the second approach, if the system size is sufficiently large. Of course, without entering into detailed numerical investigations of the relative virtues of the two approaches, we cannot make quantitative comments about the prefactor of the scaling that must taken into account in a comparison. We refer the reader to a recent article by Rasin *et al.* [40], in which the acceleration via the linear scaling has actually been demonstrated.

Comparing with the four-dimensional scheme of Miller and co-workers [33–35], we note that our model is less computationally demanding and thus seems to be more suitable, in two-dimensional (2D) simulations. On the one hand, this is a consequence of the fact that we need fewer velocities in the lattice-Boltzmann part of the model, which is entirely due to our restriction to two dimensions. On the other hand, in contrast to Miller and co-workers, we use the quantitative phase-field model of Karma and Rappel [26], convergent at larger interface thickness than approaches with only first-order asymptotics, which also reduces the computational load for a given problem, because the grid spacing is not limited by the interface thickness of the phase field.

The aforementioned scheme proposed by Rasin *et al.* [40] to solve advection-diffusion problems is even less memory-demanding and moreover allows one to simulate anisotropic diffusion. The collision matrix of this method is, however, velocity-dependent and should be computed separately for each site at each time step.

In order to test the numerics, we simulated the growth of a single needle crystal into a supercooled melt for some sets of anisotropy and supercooling values listed in Ref. [26], and verified that our code yields the same tip velocities to an accuracy of three significant digits, which approximately corresponds to the expected numerical precision. Also, we simulated the growth of dendrites at the same undercooling and anisotropy with the finite difference method of Ref. [26] and with our method, and obtained identical patterns, which means that patterns obtained by the two methods were indistinguishable by eye.

IV. PATTERN GROWTH IN A SHEAR FLOW

In this section, we will study the growth of a pattern into a horizontal shear flow near a solid wall. Comparable simulations have been performed previously by Tönhardt and Amberg [27] using a finite-element method, but they considered only dendritic growth, whereas we are mostly concerned with the influence of flow on the different known growth morphologies. A preliminary account of the results of this section has been given in Ref. [41].

Our main reason for investigating shear flow was that it is a symmetry-breaking perturbation. Let us first briefly recall some relevant aspects of the physics of dendritic growth. The capillary length is usually small, meaning that the ratio d/R in Eqs. (1) is small in comparison with the undercooling in typical experiments. In two dimensions, Ivantsov parabolas [14] are known to constitute, in the absence of surface tension, exact steady-state solutions to the equations determining the shape of a dendritic crystal for purely diffusion-limited growth [$\mathbf{U}=\mathbf{0}$ in Eqs. (1)]. It is therefore natural to assume that stationary solutions to the equations of motion have a crystal shape close to an Ivantsov parabola, if d/R is small enough. It is also well known that this assumption fails if surface tension is isotropic, i.e., $d(\theta)=d_0$, a fact that is often attributed to the singular nature of the perturbation d/R—which is a purely mathematical argument.

What happens physically is that in the case of isotropic surface tension the tip is also the coldest point of the interface, since the curvature of a needle crystal with parabolic shape (or a shape sufficiently close to parabolic) is maximum at the tip. Therefore this interface point will experience a smaller driving temperature gradient than the points in its immediate neighbourhood, rendering it vulnerable to a tip-splitting instability. As soon as we have surface tension anisotropy, the tip will not be the coldest point anymore, as the prefactor $d(\theta)$ of the curvature is smallest in the growth direction. This has a stabilizing effect on the tip, making (as one can see by going through the mathematics) steady-state near-parabolic solutions possible.

Since the discovery of doublons [42], it has been known that isotropic surface tension does *not* preclude steady-state solutions with shapes that are *far* from parabolic. Indeed, the doublon escapes the tip-splitting instability by having no tip on the symmetry axis. Due to the asymmetry of the single fingers, the points of highest curvature are, shifted from their tips to points closer to the inside of the channel separating the fingers. So even with isotropic surface tension the coldest points, tending to lag behind their immediate neighborhood, are safely moved away from the finger tips, allowing stable growth in principle.

However, when asymmetric fingers were found [43] in simulations of growth in a channel, they seemed to owe their existence to the fact that they were leaning towards the channel wall, providing them with a mirror image. It was believed that two real fingers would instead compete with one another. As soon as one would get ahead in growth, the other would lose the competition. Thus it came as a surprise that the two members of a pair could stabilize *each other*. Of course, once one of them passed the other, it would become wider, slowing down in the process, becoming more symmetric and thus susceptible to a tip-splitting instability that might result in a new pair of competing fingers—but this is not the same as stabilizing a steady state. Indeed, in systems where asymmetry of the fingers is largely suppressed by the character of surface tension anisotropy, an oscillatory scenario of this type has been observed numerically [44].

In the absence of surface tension anisotropy or with weak anisotropy, a perturbation that puts one of the fingers ahead of the other will on the one hand tend to assist its growth, because it will move its tip into a region of lower temperature, but on the other hand it will also tend to inhibit growth, because the increased tip curvature lowers the equilibrium temperature due to the Gibbs-Thomson condition. For large enough undercooling, the relative effect of the displacement will be small, as the structure is moving fast anyway, and then the surface tension effect should win, which is what seems to happen in the cooperative growth of the fingers of a doublon.

These ideas suggest that a perturbation, such as a shear flow, that disturbs the symmetry between the two fingers, might destroy their cooperative growth mode. Then doublons would not be expected to survive as (quasi)steady states in a shear flow. To answer this question is the main purpose of this section.

While some simulations of doublon-related patterns and their three-dimensional generalization using the phase-field approach have been presented in the past [45,46], they did not include convection. In fact, we are not aware of any

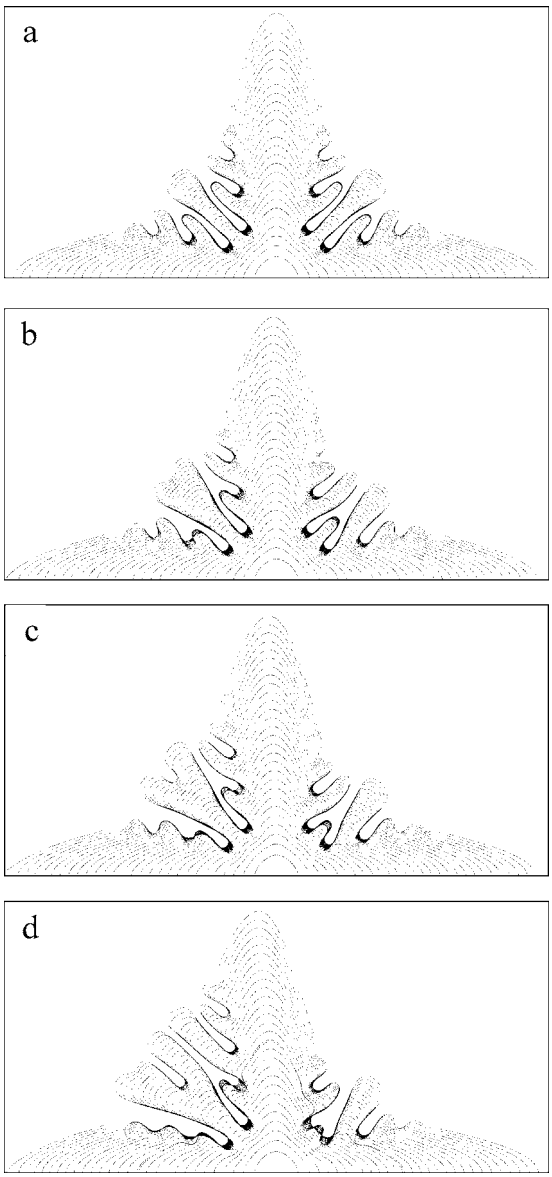

FIG. 1. Dendrite in a shear flow. Inflow from the left. Reduced velocity (a) $\bar{U}=0$, (b) $\bar{U}=0.0123$, (c) $\bar{U}=0.0247$, and (d) $\bar{U}=0.0493$.

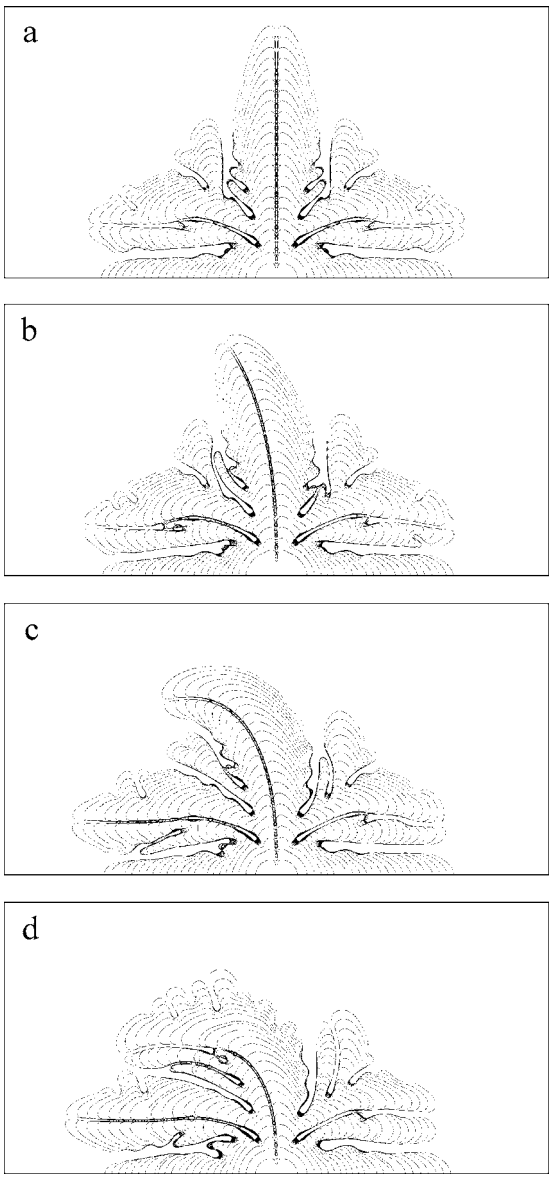

FIG. 2. Seaweed in a shear flow. Inflow from the left. Reduced velocity (a) $\bar{U}=0$, (b) $\bar{U}=0.0247$, (c) $\bar{U}=0.0493$, and (d) $\bar{U}=0.0987$.

theoretical work on doublons in the presence of convection apart from our own short publication on preliminary work [41].

In our simulation, a small seed was initially placed at the center of the bottom wall of the computational box. The boundary conditions for the phase-field equation were reflecting at the bottom, $\psi=-1$ in the inflow and at the outer boundary, and $\partial_x\psi=0$ in the outflow. The boundary conditions for the flow were $\mathbf{U}=0$ at the bottom, $\partial_x\mathbf{U}=0$ in the in- and outflow, $U_x=U_0$, $U_y=0$ at the top boundary; for the temperature we required $T=T_0$ in the inflow and at the top boundary, $\partial_y T=0$ at the bottom, and $\partial_x T=0$ in the outflow.

Results for nondimensional initial undercooling $\Delta=0.7$, $15\varepsilon=0.15$, $D=3$, $\Delta t=0.01$, $\nu=1/3$, $d_0=0.185$ and different fluid velocities are shown in Fig. 1. The Prandtl number was Pr=1.78, somewhat intermediate between the values for succinonitrile (Pr=23) and liquid metals (Pr in the percent range). Contours represent the interface of the growing pattern (points with $\psi=0$) for times up to $t=1400$, the time difference between successive contours is 50. The grid size is 2001×1000, the reduced flow velocity $\bar{U}=Ud_0/D$. In this case, the shape of the growing pattern was dendritic. Shear flow led to enhanced growth of side branches on the upstream side. The direction of the arm perpendicular to the flow was slightly modified, leading to an overall inclination of the dendrite.

Increasing the initial undercooling Δ to 0.8 with the same value of anisotropy we obtained a seaweed pattern (Fig. 2) which consists of doublons as main building blocks (here there are three of them). Boundary contours are shown for times up to $t=460$ with increments of 20.

As discussed above, it would be natural to expect a change of relative stability of two fingers of a doublon growing perpendicular to the fluid flow. The upstream finger is exposed to the colder liquid, which might lead to a gradual elimination of the second finger and the stabilization of a dendritic pattern.

In our computations, however, a qualitatively different result was observed. The perpendicular arm bends upstream and eventually becomes parallel to the flow, at least for high flow velocities. So the simulation verifies the robustness of the dynamics leading to the growth of doublons. Moreover, the alignment with respect to the flow can be understood by noting that with this alignment the two fingers tend to experience roughly the same increase in growth velocity by the flow.

With hindsight, the suppleness of doublons in adapting to the direction of an incoming flow as opposed to dendrites that tend to change their growth direction less can be easily understood. For given anisotropy, doublons grow faster than dendrites (if they exist), meaning that for given growth velocity, doublons grow at lower anisotropy than dendrites. Lower anisotropy means that the growth direction is changed more easily. Now the two simulations compared in Figs. 1 and 2 were done at the *same* anisotropy. But then the driving force Δ for the doublons was higher. It would be interesting to do simulations of both morphologies at the same anisotropy ε and undercooling Δ. To achieve this, one has to hit their (narrow) coexistence regime, the position of which is not precisely known.

V. INFLUENCE OF PARALLEL FLOW ON THE GROWTH

In the Introduction, a number of theories were mentioned [16–18] that try to establish the influence of a flow on dendritic growth. They consider a simpler configuration than a shear flow, namely an imposed flow the direction of which is (anti)parallel to the growth direction of the dendrite. In this section, we will give quantitative results on the growth velocity, tip radius, and selection parameter σ as a function of the velocity of the incoming flow for various undercoolings. For the time being, a direct comparison with the theories is not yet feasible, because the analytic formulas are valid in the range of small undercoolings, where the numerics become too time consuming.

To investigate the effects of parallel flow on the growth, the needles grown without flow in the test computations were used as initial configurations. The values of the temperature and phase fields of single dendrites were loaded. Then the flow was initialized. Boundary conditions for the flow were constant flow velocity perpendicular to the upper boundary and zero velocity (and pressure) gradients at the lower boundary, with reflecting side boundaries. The flow was allowed to evolve with a fixed configuration of the solid, and the relative velocity error was calculated at each time step as

$$U_{err} = \frac{\sum |\hat{U}_x - U_x| + |\hat{U}_y - U_y|}{\sum |U_x| + |U_y|}.$$

Here, $\hat{\mathbf{U}}$ refers to the flow velocity at the current, $\mathbf{U}$ to that at the preceding time step, the summation is over all grid nodes. The convergence condition was $U_{err} \leqslant 10^{-5}$.

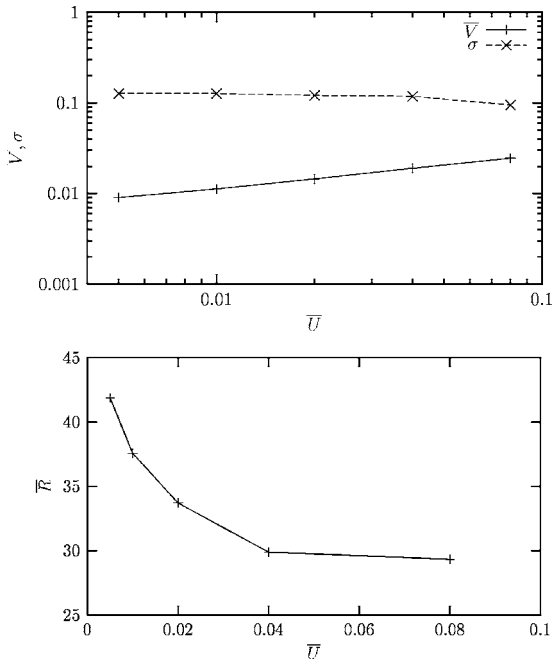

FIG. 3. Dendrite growth in parallel flow. $\Delta=0.45$, $15\varepsilon=0.75$, Pr=0.83. (a) Dependence of the reduced velocity $\bar{V}$ and selection parameter σ on the reduced flow velocity $\bar{U}$. (b) Dependence of the reduced tip radius $\bar{R}$ on the reduced flow velocity $\bar{U}$.

Then the growth of the pattern was "switched on" and continued until a steady, i.e., constant-velocity, state was reached.

Growth of a single dendritic tip was investigated for several sets of parameters, proceeding from the faster computations at relatively large undercoolings to the more interesting case of smaller undercoolings that is more amenable to analytic study. We present results here for a number of cases in Figs. 3–5 corresponding to the lower undercoolings considered, where we could observe power law dependencies (whereas the functional dependencies were more complicated at higher undercooling):

(1) $\Delta=0.45$, $15\varepsilon=0.75$, $D=4$, $d_0=0.139$, Pr=0.83,
(2) $\Delta=0.55$, $15\varepsilon=0.75$, $D=2$, $d_0=0.277$, Pr=0.83, and
(3) $\Delta=0.45$, $15\varepsilon=0.75$, $D=4$, $d_0=0.139$, Pr=5.

The dependence of the reduced tip velocity $\bar{V}=Vd_0/D$ and selection parameter $\sigma=2/\bar{R}^2\bar{V}$ on the reduced flow velocity $\bar{U}$ is shown in Fig. 3(a) (case 1), Fig. 4(a) (case 2), and Fig. 5(a) (case 3). The behavior of reduced tip radius $\bar{R}=R/d_0$ is shown in Figs. 3(b), 4(b), and 5(b).

The dendrite tip velocity increases with the increase of flow velocity, whereas the tip radius decreases. The selection parameter σ remains almost constant in some range of flow velocities ($\sigma \sim \bar{U}^{-0.04}$ in case 1, $\sigma \sim \bar{U}^{-0.08}$ in case 2, and $\sigma \sim \bar{U}^{-0.06}$ in case 3). This behavior is in accord with theoretical conclusions [16] stating that for small enough flow velocities the selection parameter itself does not change. However, the functional dependence of the Péclet number on the undercooling changes, and so do the laws determining the

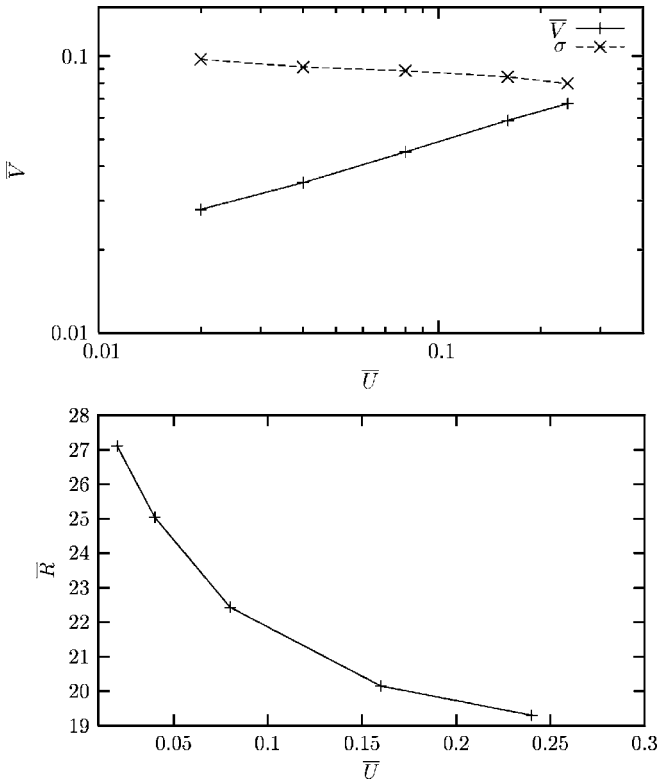

FIG. 4. Dendrite growth in parallel flow. $\Delta=0.55$, $15\varepsilon=0.75$, Pr=0.83. (a) Dependence of the reduced velocity $\bar{V}$ and selection parameter σ on the reduced flow velocity $\bar{U}$. (b) Dependence of the reduced tip radius $\bar{R}$ on the reduced flow velocity $\bar{U}$.

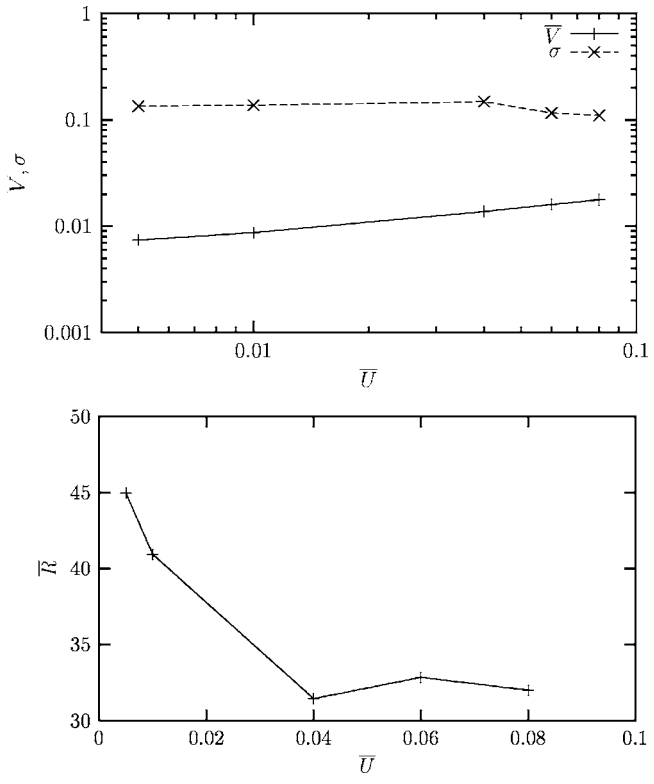

FIG. 5. Dendrite growth in parallel flow. $\Delta=0.45$, $15\varepsilon=0.75$, Pr=5. (a) Dependence of the reduced velocity $\bar{V}$ and selection parameter σ on the reduced flow velocity $\bar{U}$. (b) Dependence of the reduced tip radius $\bar{R}$ on the reduced flow velocity $\bar{U}$.

growth velocity and tip radius as a function of the undercooling. Moreover, a flow Péclet number arises as additional parameter, increasing the parameter space.

The dependence of dendrite tip velocity can be fitted as $\bar{V}\sim\bar{U}^{0.38}$ (case 1), $\bar{V}\sim\bar{U}^{0.36}$ (case 2), and $\bar{V}\sim\bar{U}^{0.32}$ (case 3). For the reduced tip radius, we also obtain compatibility with power law behaviors as function of the flow velocity according to $\bar{R}\sim\bar{U}^{-0.16}$ (case 1), $\bar{R}\sim\bar{U}^{-0.14}$ (case 2), and $\bar{R}\sim\bar{U}^{-0.13}$ (case 3). The exponents have similar values in all cases considered.

Assuming the selection parameter to be constant, simple power laws can be derived for the growth velocity and tip radius as a function of the imposed flow velocity in the limit of large Prandtl number and small undercooling ($\bar{V}\sim\Delta^{4/3}\bar{U}^{2/3}$, $\bar{R}\sim\Delta^{-2/3}\bar{U}^{-1/3}$). However, this is not the limit applicable here, so we do not expect the exponents to be relevant. It is still amusing to note that they seem to be off by roughly a factor of 2.

In dataset 3, we have increased the Prandtl number by almost an order of magnitude in comparison with dataset 1. However, even the decently large value of 5 does not lead to exponents that are closer to the theoretical predipotion than those of sets 1 and 2. Most likely this is due to the fact that our undercoolings are still too large.

Another prediction of the theory [16] is that once a threshold value of the flow velocity is exceeded, steady needle crystals do not exist anymore. This is in agreement with the observation demonstrated in Figs. 6 and 7: We find that at large flow velocities, oscillations of the tip velocity emerge, which are accompanied by enhanced growth of side branches. Here, $\Delta=0.7$, $15\varepsilon=0.15$, $D=3$, $d_0=0.185$, Pr $=1.78$. In phase-field simulations, side branching is ordinarily well suppressed after geometry effects from the initialization have died out. To obtain side branches in the asymptotic state, noise must usually be added explicitly (which is good from a theoretical point of view, since in most experiments side branches are a consequence of thermal noise), so the fact that side branches appear here without noise is quite remarkable. It points to a possible new mechanism of side branch generation (that should result in coherent side branches).

For the smaller undercoolings investigated, tip velocity oscillations did not appear, even for larger flow velocities. It should be mentioned, however, that anisotropy was much larger in those cases. Hence tip velocity oscillations and the growth of side branches look like a result of several destabilizing factors: large (undercooling and) flow velocity combined with low anisotropy. This question deserves further investigation.

VI. CONCLUSIONS

In summary, we have presented a lattice-Boltzmann model for the simulation of dendritic growth which incorpo-

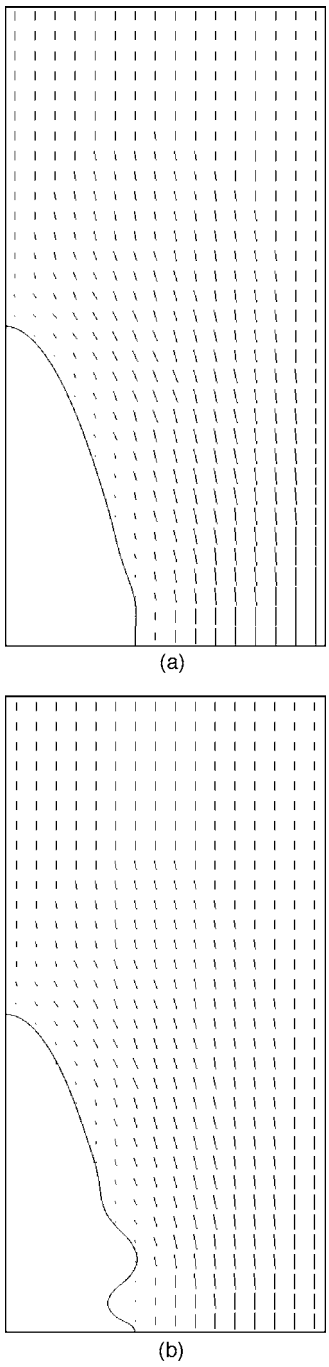

FIG. 6. Growth of side branches, $\Delta=0.7$, $15\varepsilon=0.15$. Reduced flow velocity (a) $\bar{U}=0.01$ and (b) $\bar{U}=0.04$.

rates fluid flows and thermal convection in a natural way. The method is simple to implement, numerically efficient, and well suited for parallel computing.

The simulations show that doublons behave differently from dendrites in an externally imposed shear flow. It appears that dendrites grow at a constant angle towards the incoming cold flow. This angle of inclination becomes larger as the flow speed increases, but the dendrite does not display a tendency to further modify its growth direction, once it has zeroed in on a fixed angle in a given simulation. Doublons

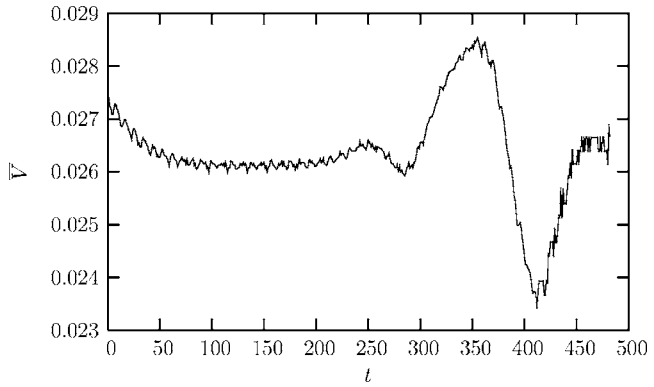

FIG. 7. Time dependence of dendrite tip velocity for the case of Fig. 6(a).

actually turn into the flow, approaching a growth direction that is antiparallel to the flow. So there is a stronger influence of the external flow on the growth of doublons than on that of dendrites.

Nevertheless, we have also seen that doublon dynamics are robust enough to survive exposure to a shear flow, which in itself is interesting, given the arguments suggesting themselves that a pair of fingers growing side by side might not survive such a symmetry-breaking perturbation.

The influence of parallel flow on the operating state of dendrite tip was investigated quantitatively (Figs. 3–5). While we are able to get the undercooling sufficiently low to obtain power law behavior as a function of the imposed flow, we are still too far from the domain of validity of analytic approximation to obtain quantitative agreement of the exponents.

Finally, our simulations have demonstrated the onset of tip velocity oscillations and an enhancement of side branching under parallel flow (Figs. 6 and 7). This raises the question of doublon stability anew, this time in a different flow configuration. Since doublons are in principle susceptible to an oscillatory instability of the two fingers, flow conditions that render dendrites oscillating might trigger this instability for doublons. We hope to report on this question in the future.

Generally speaking, we believe to have shown that the presented method of combining the phase-field and lattice-Boltzmann approaches is a viable tool for the investigation of crystal growth in the presence of convective flows. Moreover, a generalization to three-dimensional systems does not pose any problems of principle, as for both building blocks of the method their generalizability has been shown in the literature. Simulations of growth in the presence of natural thermal convection were also carried out but will be reported on elsewhere.

ACKNOWLEGMENTS

Financial support of this work by the German Research Foundation (DFG) under Grant No. FOR 301/2-1 within the framework of the research group "Interface dynamics in pattern forming processes" is gratefully acknowledged.

[1] B. Caroli, C. Caroli, B. Roulet, and J. S. Langer, Phys. Rev. A **33**, 442 (1986).
[2] M. Ben Amar and Y. Pomeau, Europhys. Lett. **2**, 307 (1986).
[3] D. I. Meiron, Phys. Rev. A **33**, 2704 (1986).
[4] D. A. Kessler and H. Levine, Phys. Rev. B **33**, 7867 (1986).
[5] A. Barbieri, D. C. Hong, and J. S. Langer, Phys. Rev. A **35**, 1802 (1987).
[6] E. Ben-Jacob *et al.*, Phys. Rev. Lett. **57**, 1903 (1986).
[7] E. Brener, H. Müller-Krumbhaar, and D. Temkin, Europhys. Lett. **17**, 535 (1992).
[8] E. Brener, K. Kassner, H. Müller-Krumbhaar, and D. Temkin, Int. J. Mod. Phys. C **3**, 825 (1992).
[9] E. Brener, H. Müller-Krumbhaar, and D. Temkin, Phys. Rev. E **54**, 2714 (1996).
[10] S. Dash and W. Gill, Int. J. Heat Mass Transfer **27**, 1345 (1984).
[11] D. A. Saville and P. J. Beaghton, Phys. Rev. A **37**, 3423 (1988).
[12] M. Ben Amar, P. Bouissou, and P. Pelcé, J. Cryst. Growth **92**, 97 (1988).
[13] R. Ananth and W. Gill, Chem. Eng. Commun. **68**, 1 (1988).
[14] G. P. Ivantsov, Dokl. Akad. Nauk SSSR **58**, 567 (1947).
[15] L. Cummings, Y. Hohlov, S. Howison, and K. Kornev, J. Fluid Mech. **378**, 1 (1999).
[16] P. Bouissou and P. Pelcé, Phys. Rev. A **40**, 6673 (1989).
[17] M. Ben Amar and Y. Pomeau, C. R. Acad. Sci., Ser. II: Mec., Phys., Chim., Sci. Terre Univers **308**, 907 (1989).
[18] R. Ananth and W. Gill, J. Cryst. Growth **108**, 173 (1990).
[19] P. Bouissou, B. Perrin, and P. Tabeling, Phys. Rev. A **40**, 509 (1989).
[20] V. Emsellem and P. Tabeling, J. Cryst. Growth **156**, 285 (1995).
[21] M. E. Glicksman, M. B. Koss, and E. A. Winsa, Phys. Rev. Lett. **73**, 573 (1994).
[22] R. Sekerka, S. Coriell, and G. McFadden, J. Cryst. Growth **171**, 303 (1997).
[23] R. Sekerka, S. Coriell, and G. McFadden, J. Cryst. Growth **154**, 370 (1995).
[24] D. Juric, in *Modeling of Casting, Welding and Advanced Solidification Processes VIII*, edited by B. Thomas and C. Beckerman (The Minerals, Metals and Materials Society, AIME, 1998), pp. 605-612.
[25] A. Karma and W.-J. Rappel, Phys. Rev. E **53**, R3017 (1996).
[26] A. Karma and W.-J. Rappel, Phys. Rev. E **57**, 4323 (1998).
[27] R. Tönhardt and G. Amberg, J. Cryst. Growth **194**, 406 (1998).
[28] C. Beckermann *et al.*, J. Comput. Phys. **154**, 468 (1999).
[29] X. Tong, C. Beckermann, A. Karma, and Q. Li, Phys. Rev. E **63**, 061601 (2001).
[30] R. Benzi, S. Succi, and M. Vergasola, Phys. Rep. **222**, 145 (1992).
[31] S. Chen and G. Doolen, Annu. Rev. Fluid Mech. **30**, 329 (1998).
[32] G. De Fabritiis, A. Mancini, D. Mansutti, and S. Succi, Int. J. Mod. Phys. C **9**, 1405 (1998).
[33] W. Miller, S. Succi, and D. Mansutti, Phys. Rev. Lett. **86**, 3578 (2001).
[34] W. Miller and S. Succi, J. Stat. Phys. **107**, 173 (2002).
[35] W. Miller, Int. J. Mod. Phys. B **17**, 227 (2003).
[36] Y. Qian, D. d'Humières, and P. Lallemand, Europhys. Lett. **17**, 479 (1992).
[37] X. Shan, Phys. Rev. E **55**, 2780 (1997).
[38] R. Almgren, SIAM J. Appl. Math. **59**, 2086 (1999).
[39] A. Kupershtokh, in *Proceedings of the 5th International EHD Workshop* (University of Poitiers, Poitiers, France, 2004), pp. 241-246.
[40] I. Rasin, S. Succi, and W. Miller, J. Comput. Phys. **206**, 453 (2005).
[41] D. Medvedev and K. Kassner, J. Cryst. Growth **275**, e1495 (2005).
[42] T. Ihle and H. Müller-Krumbhaar, Phys. Rev. E **49**, 2972 (1994).
[43] E. Brener, H. Müller-Krumbhaar, Y. Saito, and D. Temkin, Phys. Rev. E **47**, 1151 (1993).
[44] R. Guérin, J.-M. Debierre, and K. Kassner, Phys. Rev. E **71**, 011603 (2005).
[45] T. Abel, E. Brener, and H. Müller-Krumbhaar, Phys. Rev. E **55**, 7789 (1997).
[46] S. Tokunaga and H. Sakaguchi, Phys. Rev. E **70**, 011607 (2004).